*J. Fluid Mech.* (1992), *vol.* 235, *pp.* 557–577
*Printed in Great Britain*



# The motion of a buoyant cloud along an incline in the presence of boundary mixing

By Y. NOH AND H. J. S. FERNANDO
Department of Mechanical and Aerospace Engineering, Arizona State University, Tempe, AZ 85287–6106, USA

(Received 6 July 1990 and in revised form 29 July 1991)

The effects of boundary mixing on the transport of a buoyant cloud along an incline were investigated using a laboratory experiment. A fixed volume of a negatively buoyant substance (a suspension of aluminium particles or a saline solution) was introduced onto a rough inclined plane, which was submerged in homogeneous water and could make planar oscillations so as to produce turbulence. At weak turbulence intensities, the buoyant input flowed down the slope as a well-defined gravity current. As the intensity of turbulence became stronger, however, the buoyant input diffused away into the interior of the fluid. The frontal velocity of the gravity current, the density structure and the growth of the thickness of the buoyant cloud were measured, and their dependencies on the intensity of turbulence at the boundary were determined. A criterion which predicts the transition from gravity-current-dominated transport to turbulent-diffusion-dominated transport was found. Scaling arguments were developed to explain the experimental results.

## 1. Introduction

When suspended sediments are introduced into an estuary, or when heavy waste matter is discharged into coastal seas, they move down the continental slope as gravity currents. Such currents are often subjected to boundary-generated turbulence, which can modify them significantly. When the velocity of the gravity current decreases and the intensity of turbulence increases, turbulent diffusion of suspended particles in the direction normal to the slope is enhanced. Depending on the degree of boundary mixing, the suspended particles will either pollute the whole water mass by turbulent diffusion or move along the slope and spread in the benthic region. In order to understand oceanographic processes or to handle environmental waste disposal problems, it is important to predict how the suspended particles discharged onto the continental shelf are dispersed under different background conditions. In addition, the prediction of the intensity of turbidity currents along the continental slope is essential to prevent possible damage to underwater facilities (Simpson 1987).

Only a few laboratory experiments have been performed to understand the effect of background turbulence on gravity currents. Thomas & Simpson (1985) investigated the effect of oscillating grid-generated turbulence on gravity currents propagating along a horizontal plane. They found that the mixing across the surface of the current is determined by the entrainment due to the eddies of the background turbulence when $\sigma/U_f > 0.5$, whereas it approaches the normal gravity current results when $\sigma/U_f < 0.005$; here $\sigma$ is the r.m.s. velocity of the background turbulence near the surface of the current and $U_f$ is the advancing velocity of the front. Linden

& Simpson (1986) examined the destruction of a gravity current by the background turbulence induced by bubbling air from the base of the experimental tank. In this case, the gravity current was produced by a lock exchange process.

In the above-mentioned experiments the gravity currents were generated along a horizontal plane, and the methods of generation of turbulence were not representative of tidal mixing on the continental shelf. Previous studies have shown that the motion of a gravity current down a slope is appreciably different from the case where it propagates along a horizontal plane (Simpson 1987). For example, as the slope angle becomes larger ($\theta > 5°$), the motion of the current is increasingly dominated by the gravitational acceleration due to the buoyancy of the cloud rather than the pressure gradient across the front.

Furthermore, although the gravity currents driven by a density difference generated owing to dissolved material such as saline water (called 'density currents') have been used in most of the laboratory experiments, since they are easy to control and are amenable to measurement, the gravity currents generated owing to suspended particles (called 'turbidity currents') are also important in many cases. Experiments with turbidity currents (Middleton 1966; Allen 1971) show that most of their features, such as the nature of mixing at the head and the relationships between velocity, depth and density difference, are similar to those of density currents provided that the settling velocity of the suspended particles is much smaller than the r.m.s. velocity of turbulence within the gravity current. It should be noted, however, that there are characteristics intrinsic to turbidity currents such as sedimentation and erosion of particles at the bottom.

Recently, Noh & Fernando (1991) investigated the effects of boundary mixing on a continuous gravity current – called a plume – propagating along an incline. They observed that the current velocity and the density within the current decrease significantly with the intensity of the background turbulence. The changes of the entrainment mechanism across the current surface were found to be consistent with the corresponding observations of Thomas & Simpson (1985) mentioned above. As a continuation of this study, laboratory experiments were carried out to investigate the dispersion of a finite volume of a negatively buoyant substance (a suspension of aluminium particles or a saline solution) – called a thermal – under boundary-induced turbulence. The turbulence was generated by oscillating a rough inclined plane submerged in homogeneous water and the buoyant fluid was introduced onto it. The propagation of the buoyant fluid (cloud) was monitored and some properties of the cloud were measured. In §2, the experimental procedure is described, and the results of the experiments are presented in §3. An analysis of the experimental results is given in §4, and §5 concludes the paper with summary.

## 2. Experimental procedure

The experiments were conducted in a Plexiglas tank of internal dimensions $241.3 \times 27.9 \times 45.7$ cm. A Plexiglas plate of dimensions $101.6 \times 27.9$ cm was mounted inside the tank using tivar bearing guides fixed to the sidewalls so that it forms an inclined bed. The plate was connected to an oscillating mechanism. The slope of the plate was 24°, and was fixed during the experiments. In order to facilitate the production of turbulence, the surface of the plate was roughened by attaching 1 cm Plexiglas cubes to the vertices of a triangular array with sides of 5 cm. In order to minimize possible secondary flow at the junction, a thin barrier was placed parallel to the inclined plate at the intersection of the horizontal bed and the slope. Figure

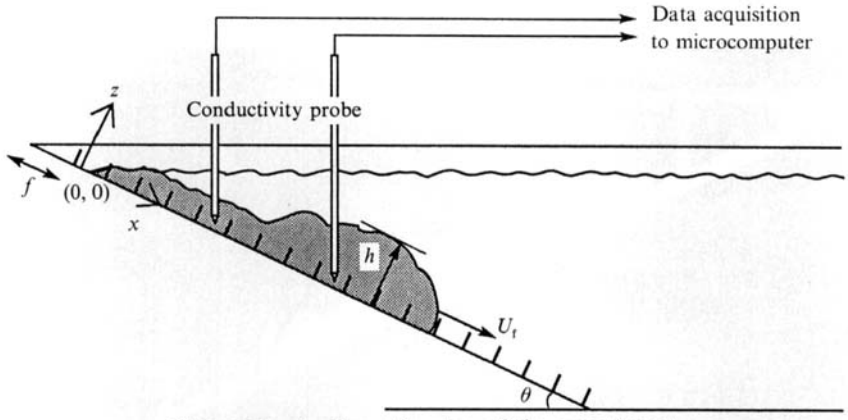


FIGURE 1. A schematic view of the experiment.

1 shows a schematic view of the experimental arrangement and the coordinate system used; the origin is at the intersection of the water surface and the slope, and $x$ and $z$ are measured parallel and normal to the slope. This experimental apparatus, which was also used by Noh & Fernando (1991), is somewhat similar to that used by Phillips, Shyu & Salmun (1986) in their boundary mixing experiments.

During the experiments, the tank was filled with fresh water to a height of 40.7 cm, and then the grid oscillations were started. After a few minutes, when the turbulence was fully established, a fixed volume (30 ml) of saline solution (density current experiment) or suspension of aluminium particles (turbidity current experiment) was released upstream of a semicircular rod located at $x = 0$ cm. The aluminium particles were filtered to yield particles with a settling velocity of $0.05 \pm 0.01$ cm s$^{-1}$. The rod was of 0.8 cm radius, and was placed to act as an obstruction to the oncoming fluid, thus distributing the heavy fluid uniformly across the width of the tank. In most cases, however, the flow was distributed over the entire width of the tank as soon as it was released, owing to the roughness elements and background turbulence, and produced a uniform flow in the spanwise direction.

A vertical sheet of intense light passing through the centre of the tank was used for flow visualization. Fluorescein dye was used for the visualization of the density currents, and the turbidity currents were self-reflected owing to the presence of aluminium particles. The flow patterns were recorded by a camera and a video recorder, and the records were used later for data analysis. In addition, the density measurements in the density current experiments were made using two conductivity probes placed at $x = 33$, 55 cm and at $z = 1.0$ cm.

The role of shear-free boundary-induced turbulence was parameterized using the eddy diffusivity $K$ near the boundary. The value of $K$ was evaluated using the following method. A small cloud of fresh water dyed with fluorescein was introduced just above the oscillating plane, and the growth of the size of the dyed cloud $l$ was measured in a large number of experiments with different oscillating frequencies. The value of $K$ was then calculated using the relation (Tennekes & Lumley 1972; Fischer *et al.* 1979)

$$\frac{1}{2}\frac{\mathrm{d}l^2}{\mathrm{d}t} = K, \tag{2.1}$$

where $t$ is the time. If it is assumed that the turbulent diffusivity can be represented by an expression of the form (cf. Phillips *et al.* 1986)

$$K = c_1 f S d, \tag{2.2}$$

(a)

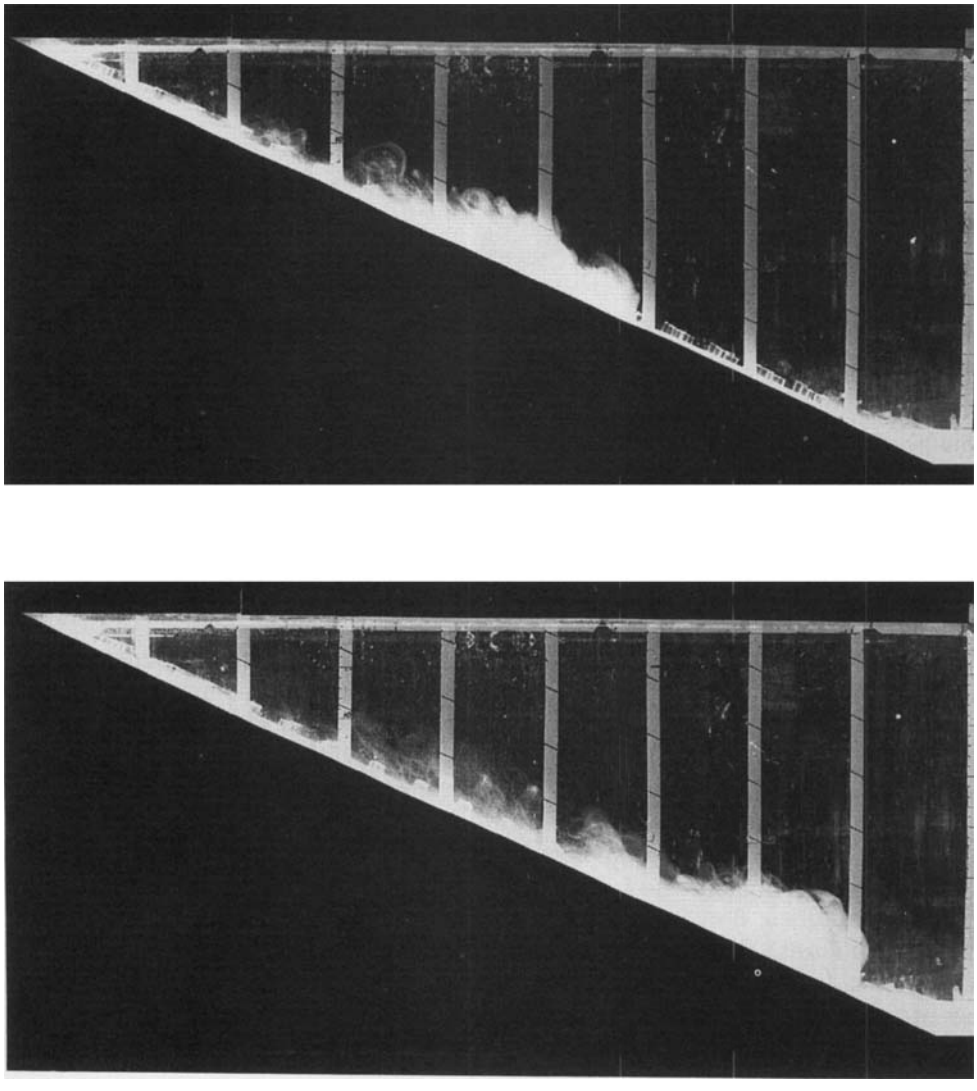

FIGURE 2(a). For caption see p. 563.

where $f$ and $S$ are the frequency and the stroke of the oscillations and $d$ is the size of roughness elements (cubes), then the measurements show that $c_1 \approx 0.27$. During the experiments, $S$ (= 1.8 cm) and $d$ (= 1.0 cm) were held fixed.

## 3. Results

### 3.1. *Qualitative observations*

Figure 2(a–d) shows the effect of different background turbulence levels on the downward transport of a fixed buoyant volume of aluminium particles with $Q$ = 70.3 cm$^3$ s$^{-2}$, where $Q$ is the total released buoyancy per unit width. The turbulent diffusivity, controlled by the frequency of the oscillation of the inclined plane, increases from (a) to (d), with $K$ = 0, 1.59, 3.37 and 5.97 cm$^2$ s$^{-1}$, respectively.

(*b*)

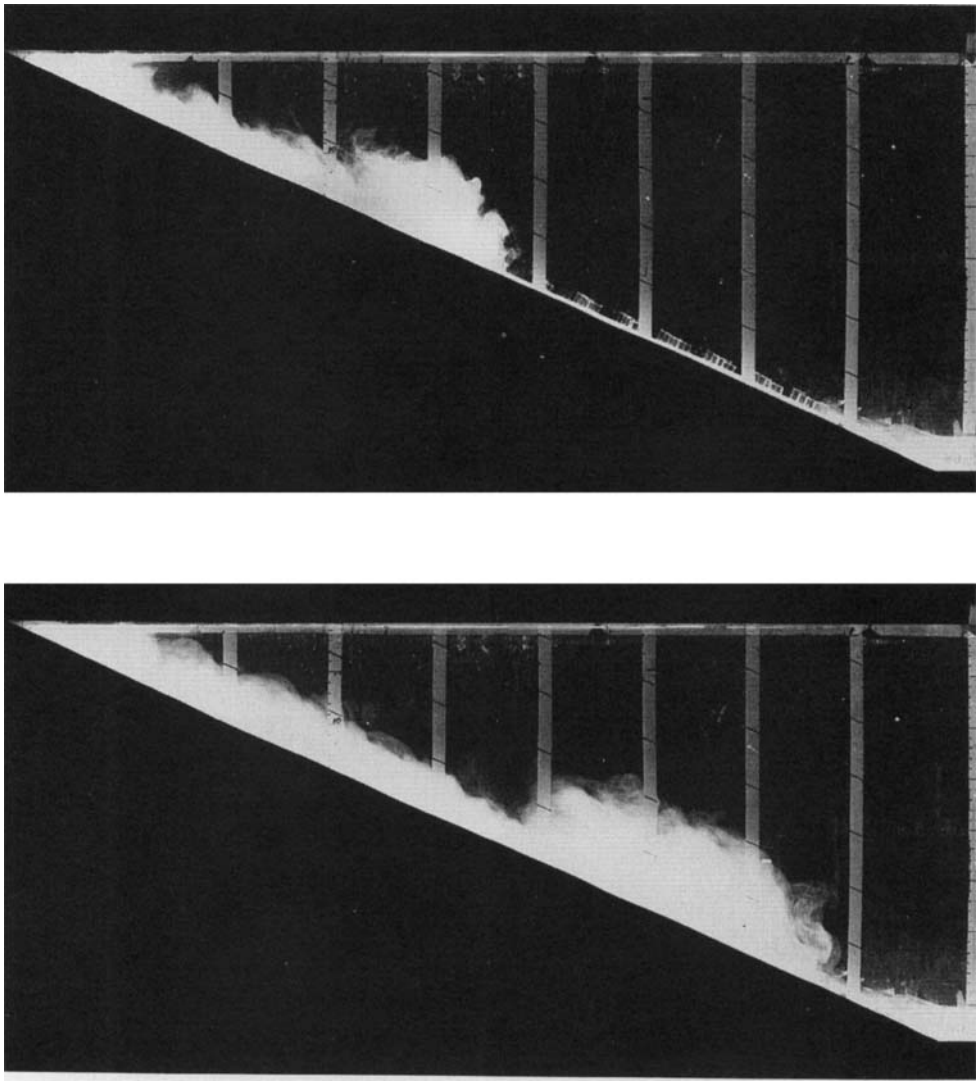

FIGURE 2(*b*). For caption see p. 563.

In the absence of background turbulence at the boundary ($K = 0$ cm$^2$ s$^{-1}$, figure 2*a*), the buoyant cloud moves down the slope with an approximately half-ellipse shape. The typical characteristics of the gravity currents, such as the sharp front and the interfacial mixing caused by Kelvin–Helmholtz instabilities, can be seen. A somewhat similar pattern is observed when the turbulence level is relatively low ($K = 1.59$ cm$^2$ s$^{-1}$, figure 2*b*), except that the thickness of the buoyant cloud grows faster and a considerable amount of the buoyant substance has been left behind. In addition, the velocity of the gravity current has decreased. When the turbulence level becomes higher ($K = 3.37$ cm$^2$ s$^{-1}$, figure 2 *c*), the front is diffused, mixing occurs over the entire surface of the current owing to turbulent diffusion and the half-ellipse cross-sectional shape of the buoyant cloud is no longer evident. At very high

(c)

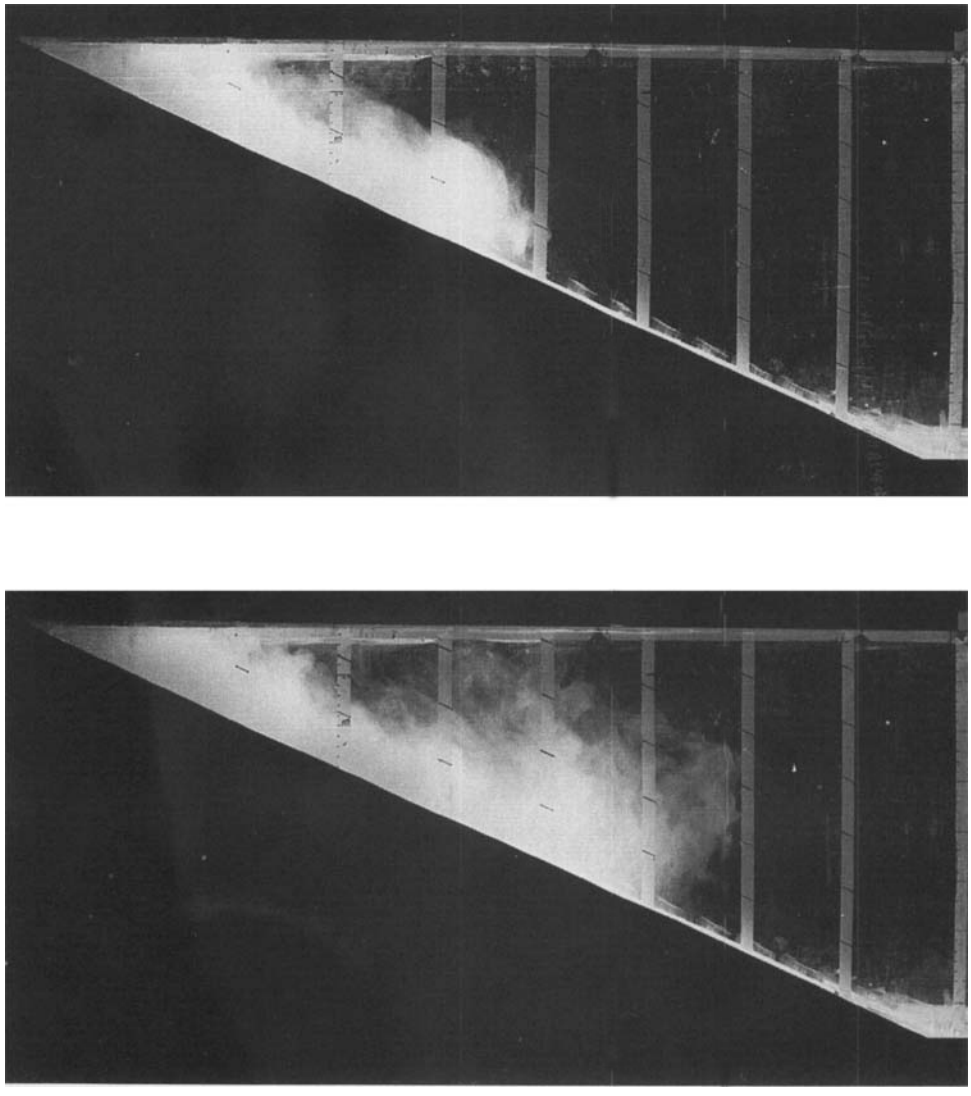

FIGURE 2(c). For caption see facing page.

turbulent intensities ($K = 5.97$ cm$^2$ s$^{-1}$, figure 2$d$), the buoyant cloud is destroyed at the outset and is dispersed as if it were a cloud of passive scalar subjected to turbulence. In this case the frontal position cannot be defined.

The corresponding density records obtained using the conductivity probes are shown in figure 3($a$–$d$). These experiments were run using the saline solution while maintaining the conditions of figure 2, except that the case of $K = 0.78$ cm$^2$ s$^{-1}$ is shown instead of $K = 0$ cm$^2$ s$^{-1}$. At small $K$ ($K = 0.78$ cm$^2$ s$^{-1}$, figure 3$a$) a buoyant cloud with a sharp front passes through the conductivity probes leaving behind a very small amount of buoyant material. As the turbulence intensity increases, a distinct tail follows the buoyant cloud although the sharp front still exists ($K = 1.59$ cm$^2$ s$^{-1}$, figure 3$b$). At still larger $K$ ($K = 3.37$ cm$^2$ s$^{-1}$, figure 3$c$), as the front arrives, a smooth peak of density can be seen. The density decreases slowly as the

(*d*)

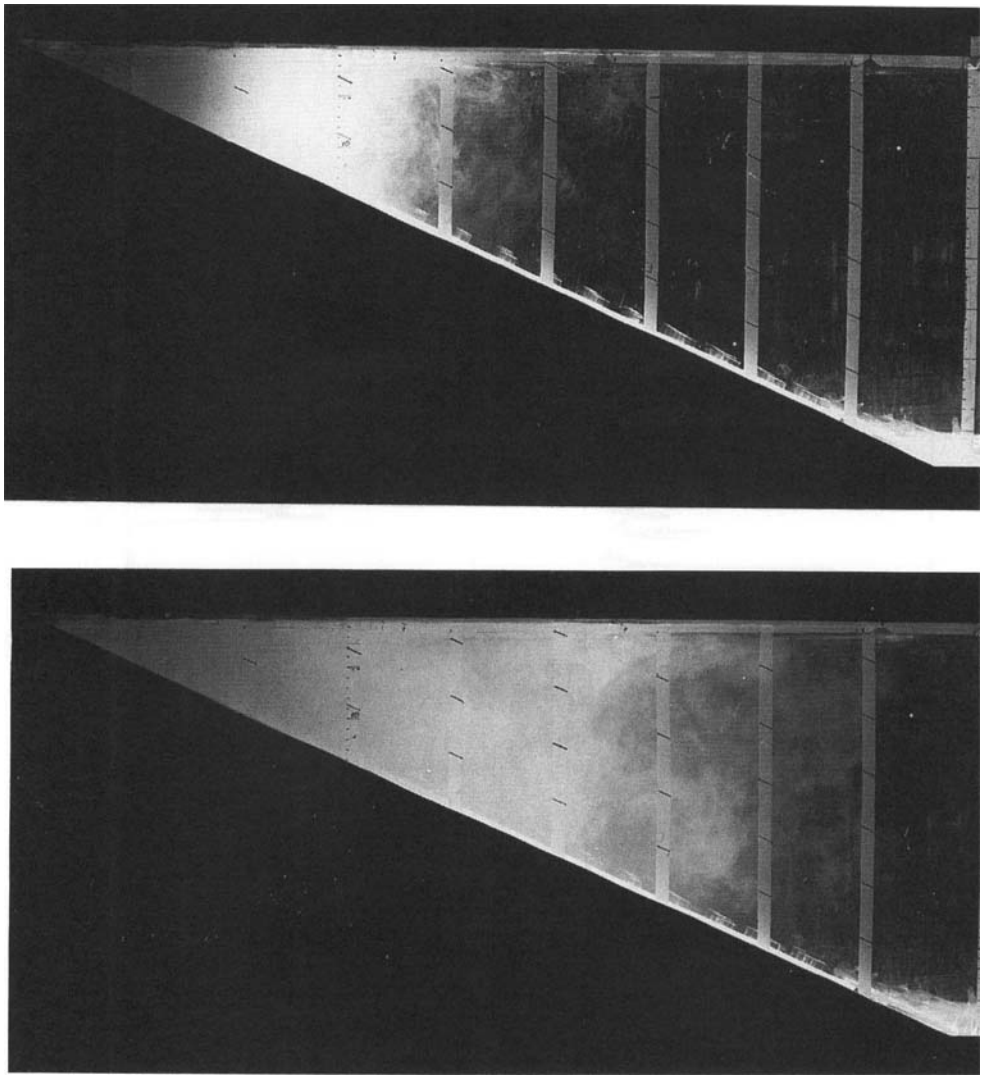

FIGURE 2. Pictures at two different times of buoyant cloud transport along an incline with different background-turbulence levels, when the same amount of buoyancy ($Q = 70.3\ \mathrm{cm^3\ s^{-2}}$, suspension of aluminium particles) is introduced: (*a*) $K = 0\ \mathrm{cm^2\ s^{-1}}$ ($t = 30,\ 60$ s); (*b*) $K = 1.59\ \mathrm{cm^2\ s^{-1}}$ ($t = 30, 60$ s); (*c*) $K = 3.37\ \mathrm{cm^2\ s^{-1}}$ ($t = 30, 60$ s); (*d*) $K = 5.97\ \mathrm{cm^2\ s^{-1}}$ ($t = 30, 120$ s).

front passes away. Figure 3(*d*) ($K = 5.97\ \mathrm{cm^2\ s^{-1}}$) shows a record typical of turbulent diffusion in which the density at a fixed point increases slowly with time.

### 3.2. *Velocity of the gravity current*

It has been found by Beghin, Hopfinger & Britter (1981) that, in the absence of background turbulence, the velocity of a two-dimensional buoyant cloud moving along an incline is given by

$$U_f = (Q \sin\theta / x_f)^{\frac{1}{2}} f_1(\theta), \tag{3.1}$$

if $x_f \gg L_0$, where $\theta$ is the slope angle, $x_f$ is the position of the gravity current front, $L_0$ is the lengthscale of the buoyant cloud at $t = 0$, and $f_i$ ($i = 1, 2, \ldots$) are functions. It has also been found that when $\theta > 5°$, $f_1(\theta) \approx 5.1$ is a constant.

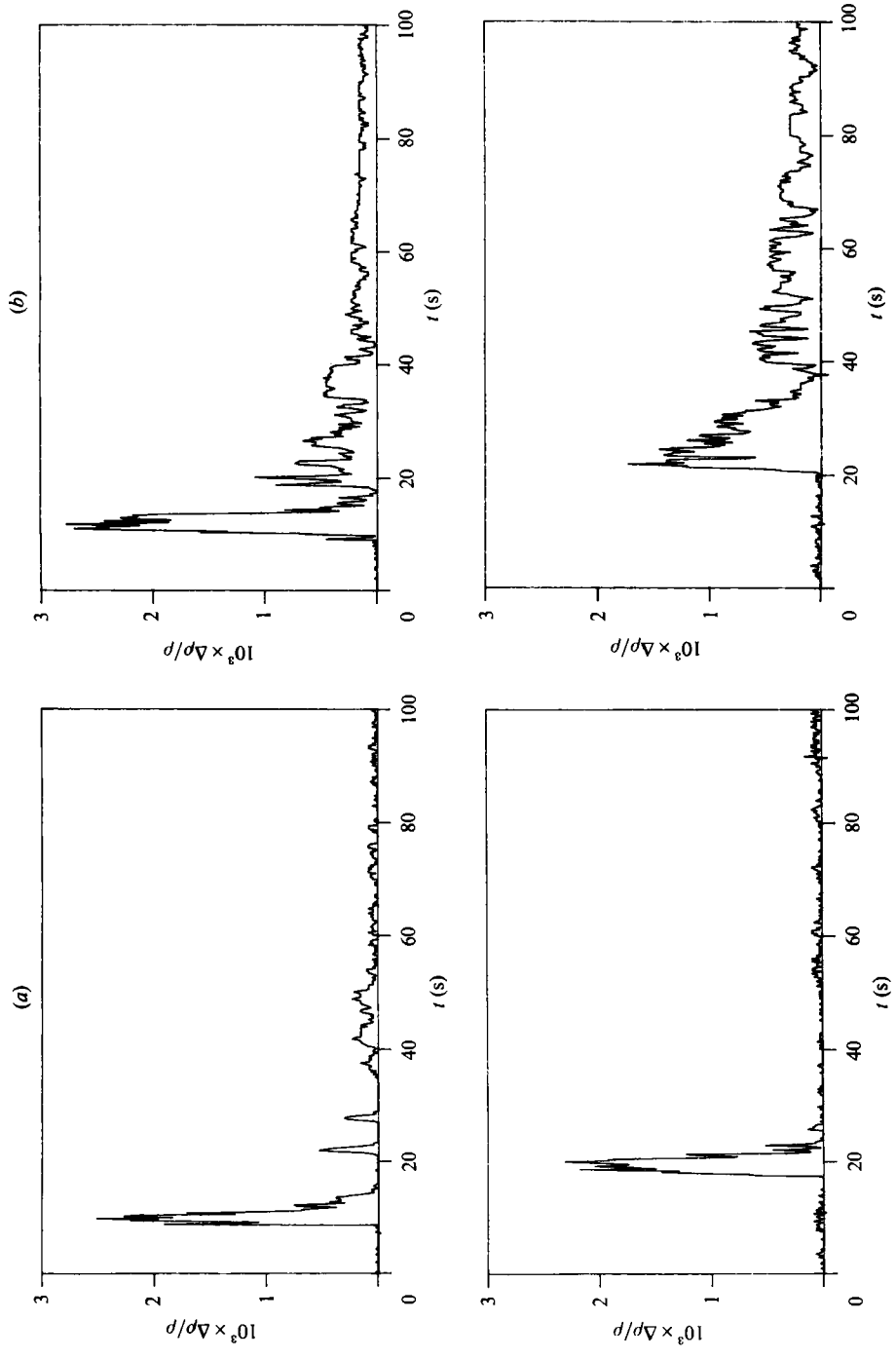
(a)
(b)
$10^3 \times \Delta\rho/\rho$
$t$ (s)
0
1
2
3
20
40
60
80
100

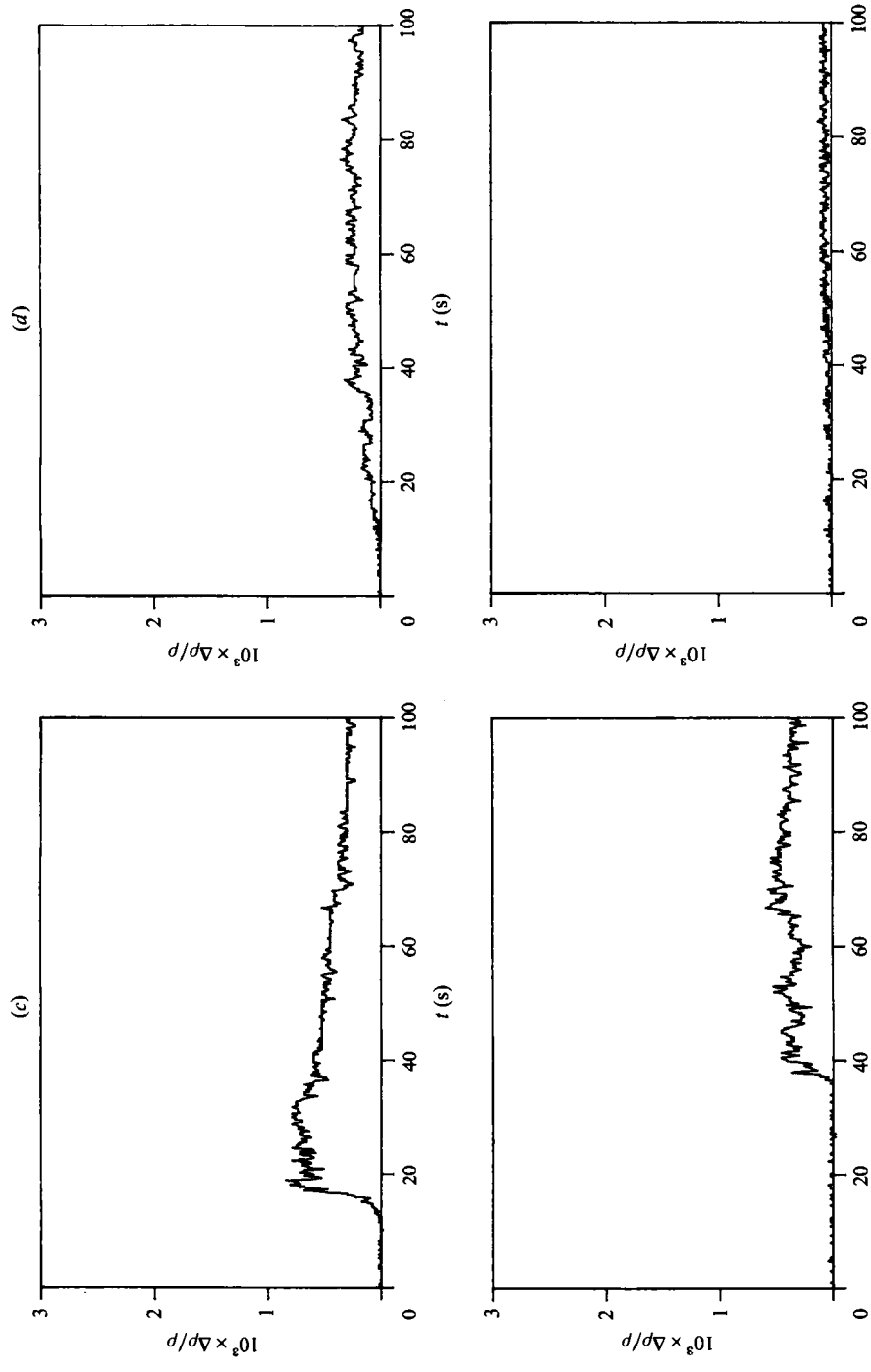


FIGURE 3. The density fluctuations measured by conductivity probes placed at $z = 1.0$ cm and $x = 33.0$ (top), 55.0 cm (bottom), when the same amount of buoyancy ($Q = 70.3$ cm$^3$ s$^{-2}$, salinity solution) is introduced: (*a*) $K = 0.78$ cm$^2$ s$^{-1}$; (*b*) $K = 1.59$ cm$^2$ s$^{-1}$; (*c*) $K = 3.37$ cm$^2$ s$^{-1}$; (*d*) $K = 5.97$ cm$^2$ s$^{-1}$.

Dimensional analysis shows that, for the cases that include the background turbulence and particle suspensions, $U_f$ can be written as

$$U_f = f_2\,(Q, x_f, K, w_s, \theta, L_0), \tag{3.2}$$

where $w_s$ is the settling velocity of the suspended particles. Hence, in the spirit of (3.1), it is possible to write, for $x_f \gg L_0$,

$$U_f = U_x f_3\,(R_x, F_x, \theta), \tag{3.3}$$

where

$$U_x = (Q \sin\theta / x_f)^{\frac{1}{2}}, \tag{3.4}$$

$$R_x = K/(Q x_f \sin\theta)^{\frac{1}{2}}, \tag{3.5}$$

$$F_x = w_s/(Q \sin\theta / x_f)^{\frac{1}{2}}. \tag{3.6}$$

Note that in (3.4)–(3.6), $Q\sin\theta$ is used instead of $Q$ in view of the fact that the streamwise component of the gravitational acceleration is reduced to $g\sin\theta$ (see (4.1) in §4).

When $\theta$ = constant and $w_s = 0$, as in the case of density currents, (3.3) takes the form

$$U_f = U_x f_4\,(R_x), \tag{3.7}$$

and for the case of turbidity currents with constant $\theta$, it becomes

$$U_f = U_x f_5\,(R_x, F_x). \tag{3.8}$$

In the present experiment, the velocity of gravity currents was measured using two techniques. In the first method, the front velocity $U_f$ was measured using video records taken at 22 cm intervals or photographs taken at 20 s intervals. In order to avoid possible complications caused by the arrival of the current at the bottom and to assure that $x_f \gg L_0$, the data were taken only in the range $33 < x_f < 77$ cm. In the second method, the velocity $U_m$ was obtained by measuring the time between the appearances of maximum density recordings of the two conductivity probes placed at $x = 33$ and 55 cm. In all cases, the calculated velocity was considered as that corresponding to the midpoint between two measurement points. When the boundary mixing is strong, both the well-defined front and the density peak disappear (see, for example, figures 2*d* and 3*d*), owing to the turbulent diffusion. In this case, it is impracticable to locate either $x_f$ or $x_m$, where $x_m$ is the position of the density peak. When it is possible to measure $U_f$ and $U_m$, the uncertainties in the measurements were estimated to be within $\pm 0.1$ cm s$^{-1}$. Since the space and/or time intervals used for the measurements of $U_f$ or $U_m$ (22 cm and 20 s) are rather large, it is possible to expect a certain amount of error in the measurements in view of the decelerating nature of the flow. Nevertheless an error analysis indicates that the typical uncertainty introduced owing to the decelerating nature of the flow is $10^{-3}$ cm s$^{-1}$, which is much smaller than that in the measurements of $x_f$.

As in Beghin *et al.* (1981), the currents accelerated rapidly after the release and then decelerated slowly. It was evident from the measurements with smaller length/time intervals that the currents were clearly in the decelerating stage when $x_f > 33$ cm. Figures 4(*a*) and 4(*b*) illustrate the behaviour of the functions $f_4$ and $f_5$ for density and turbidity currents, respectively. The data obtained from the photographic and conductivity records are included in figure 4(*a*). Note that if the front is sharp (small $R_x$), $x_m$ and $x_f$ are coincident, because in this case the maximum density of the current occurs at the front. No noticeable differences between $U_f$ and $U_m$ are found, and the current velocity $U_f/U_x$ (or $U_m/U_x$) is shown to decrease with

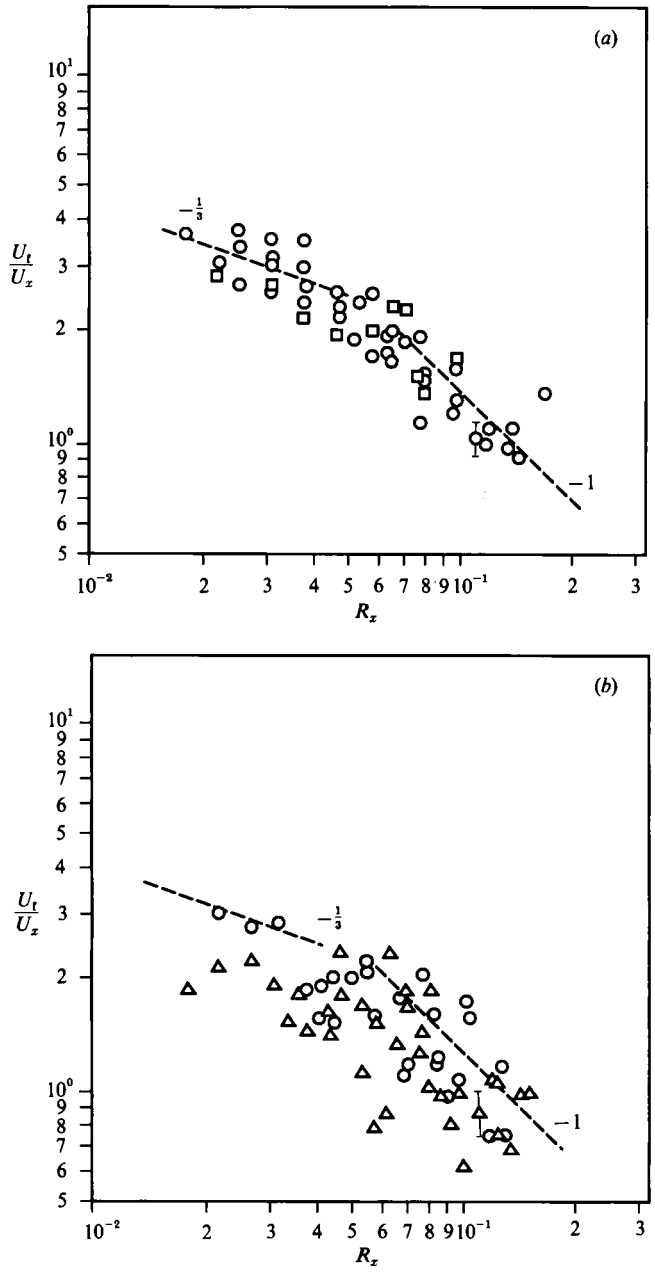


FIGURE 4. (*a*) $u_f/U_x$ (○) and $U_m/U_x$ (□) *vs.* $R_x$ from the data (*b*) $U_f/U_x$ *vs.* $R_x$ for the turbidity currents. The data are split into two groups according to the value of $F_x$ (○, $F_x < 0.06$; △, $F_x > 0.06$).

the intensity of boundary mixing. An analysis of the motion of the buoyant cloud, which will be given in §4, predicts that the relationship between $U_f/U_x$ and $R_x$ is given by

$$U_f/U_x \propto R_x^{-\alpha}, \tag{3.9}$$

where $\alpha$ increases from $\frac{1}{3}$ at small $R_x$ to 1 at large $R_x$. Figure 4(*a*) shows a good agreement between the predictions and the experimental results. Further, it was

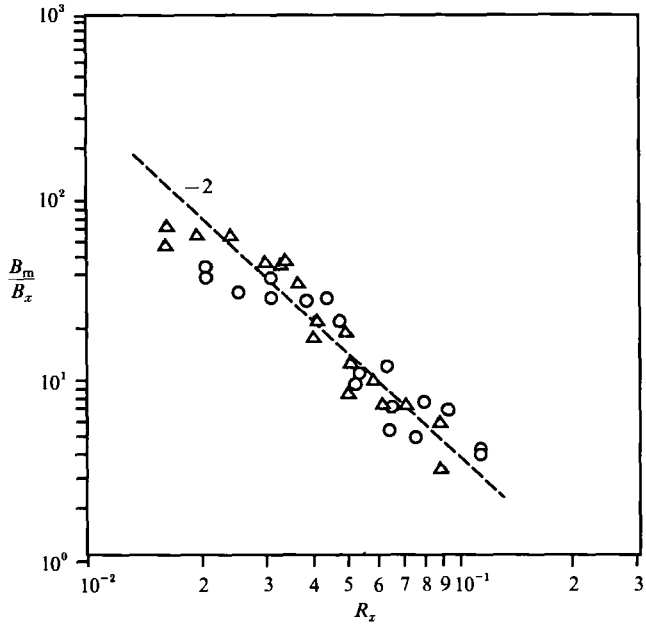


FIGURE 5. $B_m/B_x$ *vs.* $R_x$ for density-current experiments. The conductivity probes were at $z = 1.0$ cm and $x = 33$ cm (○) and 55 cm (△).

observed that $U_f/U_x \approx 4.5$, when $R_x = 0$, i.e. the case with no background turbulence. This is somewhat smaller than the value 5.1 obtained by Beghin *et al.* (1981). It is plausible that the drag due to the roughness elements on the bed and the turbulence of their wakes have a retarding effect on the current velocity.

In order to accommodate the fact that $U_f/U_x$ depends on $R_x$ and $F_x$ for turbidity currents, in figure 4(*b*) the data are divided into two groups according to the value of $F_x$ ($F_x < 0.06$; $F_x > 0.06$). The data show considerable scatter, but suggest that the current velocity decreases as the buoyant cloud loses its buoyancy owing to the settling of particles at large $F_x$.

### 3.3. *The density variation*

Dimensional analysis further shows that the maximum buoyancy within the buoyant cloud $B_m$ is determined by

$$B_m = f_6(Q, x_m, K, w_s, \theta), \tag{3.10}$$

$$= B_x f_7(R_x, F_x, \theta), \tag{3.11}$$

at $x_m \gg L_0$, where

$$B_x = Q/x_m^2. \tag{3.12}$$

When $\theta$ = constant and $w_s = 0$, (3.12) becomes

$$B_m = B_x f_8(R_x). \tag{3.13}$$

The density measurements, as shown in figure 3, were used to evaluate $B_m$, which is the maximum buoyancy at the locations of the conductivity probes. As for $U_m$, the measurement of $B_m$ in the turbulent-diffusion-dominated regime was difficult. Figure 5 shows the variation of $B_m/B_x$ with $R_x$, for $F_x = 0$. Since, in most cases, the vertical ($z$) positions of the conductivity probes are much smaller than the height of the buoyant cloud and the density tends to be uniform near the boundary owing to boundary mixing, $B_m$ can be regarded as the buoyancy at the bottom. Note that

$B_m/B_x$ shows a consistent relationship to $R_x$ over the range of experimental parameters,

$$B_m/B_x \propto R_x^{-\beta}, \tag{3.14}$$

where $\beta \approx 2$, except for small values of $R_x (R_x < 0.03)$ where $\beta$ is smaller.

### 3.4. *The growth of the thickness of the buoyant cloud*

The growth of the maximum thickness of the buoyant cloud $h^*$ with time was measured for different $K$ and $Q$ and the results are shown in figure 6 $(a, b)$. It should be noted, however, that the measurements are somewhat subjective (up to $\pm 1$ cm) because of the contorted and diffused nature of the interface. Nevertheless, the results clearly show that, for a given $Q$, $\mathrm{d}h^*/\mathrm{d}t$ increases with $K$ (figure 6$a$), whereas $\mathrm{d}h^*/\mathrm{d}t$ does not show significant dependence on $Q$ when $K$ is constant (figure 6$b$). This suggests that the growth of the buoyant cloud is determined by the background turbulence, as

$$h^* = (Kt)^{\frac{1}{2}}, \tag{3.15}$$

in accordance with (2.1) for all cases considered, except for the case $K = 0$.

From the regression of the data of figure 6, it is possible to estimate the initial height of a buoyant cloud $h_0^*$ given by

$$h_0^* = h^*(t = 0), \tag{3.16}$$

as $h_0^* \approx 1$ cm.

Measurements made with a laser-Doppler velocimeter showed that the intensity of boundary-induced turbulence $\sigma$ of the present experiment, expressed as its value at $z = 1.5$ cm, is well represented by the expression $\sigma = 0.3fS$ (Noh & Fernando 1991). The range of parameters used for the present studies were $1 < \sigma < 4$ cm$^{-1}$ and $0.3 < \sigma/U_f < 8$; this suggests that, according to Thomas & Simpson's (1985) criterion given in § 1, most of the experiments are dominated by mixing due to the background turbulence. In particular, when the stratification at the current surface is weak (for example, when the Richardson number $B_m h^* \cos\theta/\sigma^2 \sim 1$ as in the present experiments), the growth of the turbulent cloud can be described using the diffusion of passive scalars (Turner 1973). When $K = 0$, however, the growth of $h^*$ is determined by the entrainment due to the shear stresses at the current surface.

### 3.5. *Transition from the gravity current to the turbulent diffusion*

Close examination of the experimental results (figures 2 and 3) indicates that the transport of a buoyant cloud along the incline, subjected to boundary mixing, can be divided into three distinct regimes: (i) the 'gravity current' regime (figures 2$a, b$ and 3$a, b$); (ii) the 'mixed' regime (figures 2$c$ and 3$c$); and (iii) the 'turbulent diffusion' regime (figures 2$d$ and 3$d$).

The following characteristics of the flow were typical in these regimes: (i) The gravity current has a sharp front and a distinct half-ellipse cloud shape; the density variation across the front shows a sharp peak and a rapid fall off (the 'gravity current' regimes). (ii) The gravity current has a diffused front and no distinct half-ellipse cloud shape; the density variation across the front shows a smooth peak and a long tail behind it (the 'mixed' regime). (iii) The material is dispersed over the entire depth of the fluid column, and, at most, a very weak downward current is observed; the density record at a fixed point continuously increases with time (the 'turbulent diffusion' regime).

Unlike the case of gravity currents generated by lock exchange studied by Linden & Simpson (1986), a change of the 'regime' of the flow was not observed during a

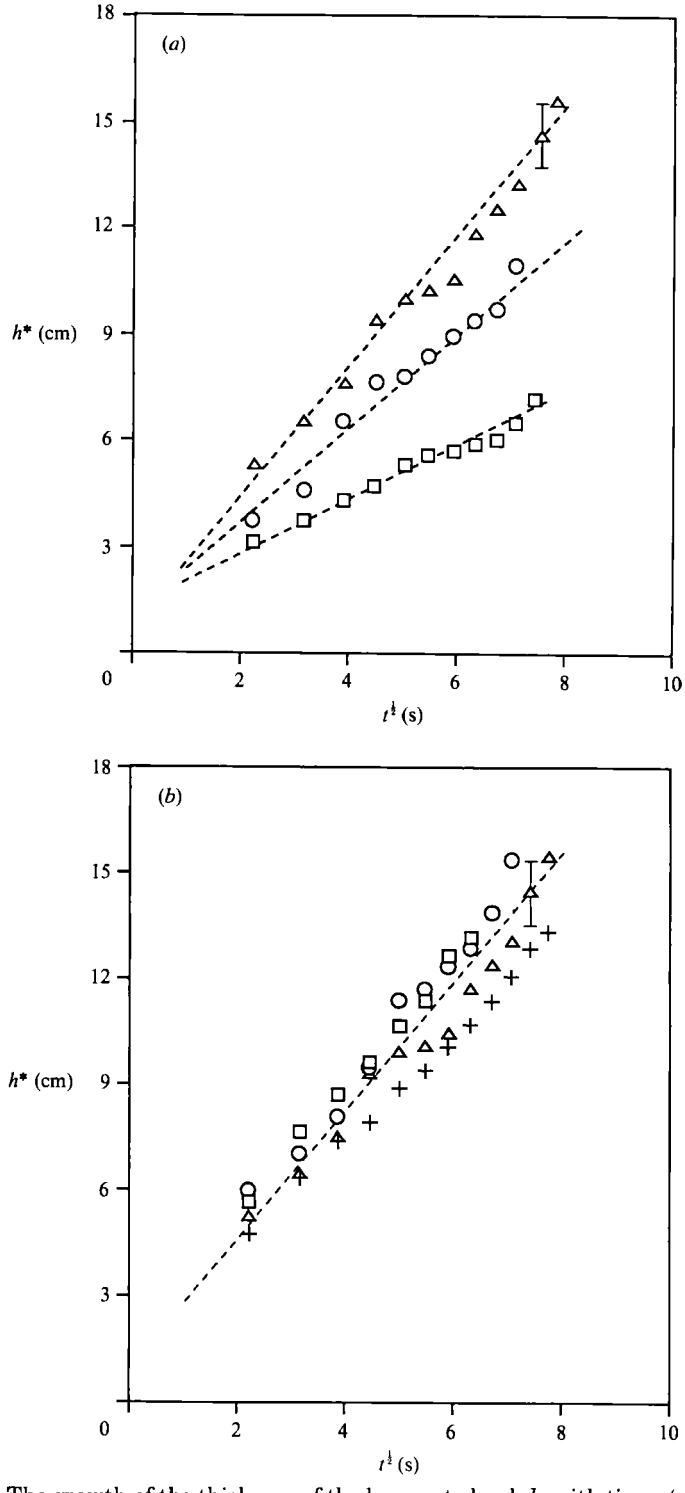


FIGURE 6. The growth of the thickness of the buoyant cloud, $h$, with time: (*a*) $Q = 70.3$ cm$^3$ s$^{-2}$; □, $K = 0$ cm$^2$ s$^{-1}$; ○, $K = 0.96$ cm$^2$ s$^{-1}$; △, $K = 2.81$ cm$^2$ s$^{-1}$. (A suspension of aluminium particles was used to generate $Q$.) (*b*) $K = 2.81$ cm$^2$ s$^{-1}$; +, $Q = 35.1$ cm$^3$ s$^{-1}$; △, $Q = 70.3$ cm$^3$ s$^{-2}$; ○, $Q = 105.4$ cm$^3$ s$^{-2}$, □, $Q = 210.7$ cm$^3$ s$^{-2}$.

given experiment. The transition from gravity current to turbulent diffusion regime is governed by the turbulent Péclet number $Pe_t$, which signifies the ratio of the transport by the advection following the gravity current to that by the turbulent diffusion. At large $Pe_t$, the gravity current transport dominates whereas the turbulent diffusion is important at small $Pe_t$. As shown in Appendix A, in the present experiment, $Pe_t$ increases as the front propagates in the gravity current regime, but it decreases with $x_f$ in the turbulent diffusion regime. Therefore it is unlikely that the transition between the regimes can occur during a given experiment. The criteria for different flow regimes are then determined by the initial conditions, characterized by $R_0$ ($\equiv K/(QL_0 \sin\theta)^{\frac{1}{2}}$), where $L_0$ can be determined by $L_0 = V^{\frac{1}{3}}$, and $V$ being the released volume of a buoyant cloud per unit width. Note that the value of $L_0$($\approx$ 1.0 cm) coincides with the experimental value $h_0^*$ of (3.16).

By analysing a large number of experiments with different $K$ and $Q$, it was possible to find criteria that divide the three regimes. The transition from 'gravity current' to 'mixed' regime was estimated to occur at $R_0 \approx 0.5 \pm 0.1$ while the transition from a 'mixed' to a 'turbulent diffusion' regime appeared at $R_0 \approx 0.9 \pm 0.1$. It was often observed, however, that a relatively sharp front appears at the initial accelerating stage during the mixed regime ($0.5 < R_0 < 0.9$).

## 4. Analysis

The depth-averaged momentum equation describing the motion of a buoyant cloud along the incline, in the presence of background turbulence, is given by

$$\frac{\partial}{\partial t}(Uh)+\frac{\partial}{\partial x}(S_1 U^2 h) = -\frac{\partial}{\partial x}(S_2 B h^2 \cos\theta)+B h \sin\theta+K\frac{\partial^2}{\partial x^2}(Uh)-K\frac{\partial U}{\partial z}\bigg|_{z=0}, \quad (4.1)$$

where $U$ ($B$) is the depth-averaged current velocity (density) and the $S_i$ ($i = 1, 2$) are profile constants (for the derivation, see Appendix B). The terms on the right-hand side of (4.1) represent, respectively, the pressure force on the cloud due to the change of its thickness, the buoyancy force responsible for accelerating the cloud, and the turbulent frictional drag. In the present work, $K$ is assumed to be determined by the background turbulence level, and the value of $K$ is regarded as constant in the boundary region, as is evident from figure 6. This is a reasonable assumption except for the case where the turbulence is significantly affected by the shear stresses induced by the current and the stratification of the fluid.

An equation similar to (4.1) has been used to describe the motion of gravity currents along an incline (Ellison & Turner 1959; Parker, Fukushima & Pantin 1986). It is also noted that (4.1) can be reduced to the thermal theory used by Beghin *et al.* (1981), if $K = 0$ and the pressure term is neglected (see Appendix C).

As suggested by Turner (1973) and Beghin *et al.* (1981), the pressure term is relatively unimportant when $\theta > 5°$, and the motion of the buoyant cloud will be determined mainly by the balance between inertial, buoyancy and frictional forces. It is also expected that the friction due to the streamwise velocity gradient is small compared with the bottom friction. The streamwise integral of each term in (4.1) over the buoyant cloud can then be estimated as

$$\text{inertial term}: I \sim S_1 U^2 h, \quad (4.2)$$

$$\text{buoyancy term}: G \sim BhL \sin\theta \sim Q \sin\theta, \quad (4.3)$$

$$\text{friction term}: F \sim KUL/\delta, \quad (4.4)$$

where $h$ and $L$ are the vertical and horizontal scales of the buoyant cloud and $\delta$ is the lengthscale of the turbulent boundary layer.

It is reasonable to assume that, regardless of the local dynamical conditions, the lengthscales $h$ and $\delta$ are of the same order, since they are imposed by the diffusion due to background turbulence, i.e.

$$h \sim \delta \sim (Kt)^{\frac{1}{2}} \sim (Kx/U)^{\frac{1}{2}} \tag{4.5}$$

and

$$L/h \sim \text{constant } (= S_4). \tag{4.6}$$

To a certain extent these assumptions are corroborated by the results of §3.4 (figure 6).

It is possible to predict the flow for the cases where $I/F \sim (S_1/S_4)\, Uh/K \gg 1$ and $I/F \ll 1$. In the former case, corresponding to small $R_x$, the motion of a buoyant cloud is determined by a balance between inertial and buoyancy forces. This leads to the relation

$$S_1 U^2 h \sim Q \sin\theta, \tag{4.7}$$

or

$$U/U_x \propto R_x^{-\frac{1}{3}}, \tag{4.8}$$

using (4.5).

On the other hand, when $I/F \ll 1$, corresponding to large $R_x$, the motion of the buoyant cloud will be determined by the balance between buoyancy and frictional forces. In this case, the relation

$$S_4 UK \sim Q \sin\theta, \tag{4.9}$$

or

$$U/U_x \propto R_x^{-1} \tag{4.10}$$

is obtained.

During the present experiments, the values of $U$, $H$ and $K$ were varied over the ranges, $0.5 < U < 5.0$ cm, $5 < H < 15$ cm and $1 < K < 6$ cm$^2$ s$^{-1}$. If $S_1 = 0.5$ (see Appendix C) and $S_4 \approx 3$ for $\theta = 24°$ (Beghin *et al.* 1981, see also figure 2), it gives the range $0.1 < I/F < 5.0$. The experimental results presented in figure 4 show that $U_f/U_x$ varies as $U_f/U_x \propto R_x^{-\frac{1}{3}}$ at small $R_x$ ($R_x < 0.03$), and $U_f/U_x \propto R_x^{-1}$, for large $R_x$ ($R_x > 0.08$), in accordance with (4.8) and (4.10).

It is important at this point to note that the parameters $I/F$, $Pe_t$ and $R_x$ are not independent, but are related to each other. The value of the ratio $I/F$ can be related to the turbulent Péclet number $Pe_t$ as

$$\frac{I}{F} \sim \frac{S_1}{S_4}\frac{Uh}{K} \sim 0.17\, Pe_t. \tag{4.11}$$

Using (3.7) and (4.5), it is again possible to relate $Pe_t$ to $R_x$ as

$$Pe_t \sim [f_4(R_x)/R_x]^{\frac{1}{2}}. \tag{4.12}$$

The conservation of mass implies that

$$BhL \sim Q \sim \text{constant}, \tag{4.13}$$

which, with (4.5) and (4.6), yields

$$B \propto \frac{Q}{Kx/U}. \tag{4.14}$$

If the relations (4.8) and (4.10) are used to estimate $U$ in (4.14), it is possible to obtain

$$B/B_x \propto R_x^{-\frac{4}{3}} \quad \text{for} \quad I/F \gg 1 \tag{4.15}$$

and $$B/B_x \propto R_x^{-2} \quad \text{for} \quad I/F \ll 1. \tag{4.16}$$

Figure 5 shows, however, that the results follow (4.16) throughout the entire range of $R_x$, except at very small $R_x$ ($R_x < 0.03$) where $\beta$ becomes smaller. The reason for this can be explained by considering the profiles of $B$ at different $R_x$ values. At small $R_x$, the profiles show a sharp peak whereas they tend to become smoother at large $R_x$ (see figure 5). Consequently, (4.13), which is based on the similarity of the profiles, ceases to be valid at small $R_x$, and $B/B_x$ shows a more rapid decrease with $R_x$ than predicted by (4.15). On the other hand, at large $R_x$ the profiles are smooth and are expected to maintain similarity, thus satisfying (4.16).

It is also important to note that (4.1) and (4.5) are no longer valid in the turbulent-diffusion regime. Here, the boundary-layer assumption used in deriving (4.1) is not possible (see Appendix B) and $h$ is determined by the water depth $H$.

## 5. Summary

Experiments were carried out to investigate how a fixed volume of negatively buoyant material (saline solution or suspended aluminium particles) is dispersed above an incline of $\theta = 24°$ in the presence of boundary mixing. Simple scaling arguments were presented to explain the experimental results.

Three regimes of fluid motion were identified for the experiments, namely, gravity-current dominated, mixed, and turbulent-diffusion dominated. During a given experiment, a transition between regimes was not found and the nature of the flow was determined by the parameter $R_0 = K/(QL_0 \sin\theta)^{\frac{1}{3}}$, where $L_0 = V^{\frac{1}{2}}$ and $V$ is the released volume of a buoyant material per unit width. Criteria predicting the gravity-current regime ($R_0 < 0.5$) and the turbulent-diffusion regime ($R_0 > 0.9$) were proposed.

In the gravity-current and mixed regime ($R_0 < 0.9$), the buoyant cloud, when it is released from the rest, accelerates quickly to the maximum velocity, and then decelerates slowly. The frontal velocity $U_f$ was found to decrease with boundary mixing as $U_f/U_x \propto R_x^{-\alpha}$, where $\alpha$ increases with $R_x$ from $\alpha = \frac{1}{3}$ at small $R_x$ ($R_x < 0.03$) to $\alpha = 1$ at large $R_x$ ($R_x > 0.08$); here $U_x = (Q \sin\theta/x_f)^{\frac{1}{3}}$ and $R_x = K/(Qx_f \sin\theta)^{\frac{1}{2}}$. The effects of particle settling, which become important when the boundary mixing is weak, were also investigated. The maximum density of the buoyant cloud $B_m$ was found to depend on the intensity of boundary mixing as $B_m/B_m \propto R_x^{-\beta}$, where $\beta \approx 2$ when $R_x > 0.03$; here $B_x = (Q/x_m^2)$. In the presence of boundary mixing, the thickness of the buoyant cloud was found to grow as $dh/dt \approx (Kt)^{\frac{1}{3}}$, independent of $Q$.

During the turbulent diffusion regime ($R_0 > 0.9$), the buoyant cloud is destroyed from the onset. The induced buoyant material is dispersed over the entire water column and is diffused away into the interior of the fluid by the background turbulence.

The authors wish to thank Professor D. F. Jankowski for his careful comments and suggestions on the paper. During the period of preparation of this paper, the authors were supported by the Office of the Naval Research (Arctic and Small-scale Oceanography Programs) and the National Science Foundation.

## Appendix A. Discussion on the transition between a gravity-current state and a turbulent-diffusion state during an experiment

For the experiments in the gravity-current regime, the turbulent Péclet numbers $Pe_t$ is given by

$$Pe_t = \frac{Uh}{K}, \tag{A 1}$$

which can be shown to be equivalent to

$$Pe_t \sim \frac{U(Kx_f/U)^{\frac{1}{2}}}{K} \sim R_x^{-(1+\alpha)/2}, \tag{A 2}$$

where (3.4), (3.9) and (4.5) have been used. Since $R_x$ decreases with increasing $x_f$, $Pe_t$ is expected to increase during an experiment.

For experiments that are dominated by the turbulent diffusion, the appropriate lengthscale is the depth of the water layer $H$. Here the flow configuration is similar to that of the lock exchange problem studied by Linden & Simpson (1986). They suggested a criterion for the transition from the gravity current regime to the turbulent diffusion regime as

$$\frac{K}{(BH)^{\frac{1}{2}}H}\frac{x_f}{H} > 0.08. \tag{A 3}$$

Since $K$ and $H$ remain constant during their experiment, $Pe_t$ decreases with $x_f$ because of the reduction of $U$; the latter is expected to decrease owing to the increased frontal thickness and consequent decrease in the horizontal pressure gradient. From (A 3), the velocity scale in the turbulent diffusion regime can be inferred as

$$U \sim (BH)^{\frac{1}{2}}(L_0/x_f) \sim (Q/x_f)^{\frac{1}{2}}(L_0/x_f), \tag{A 4}$$

and the turbulent Péclet number becomes

$$Pe_t \sim \frac{K}{(Q/x_f)^{\frac{1}{2}}(L_0/x_f)\,x_f \sin\theta}, \tag{A 5}$$

$$\sim \frac{K}{(Q/x_f)^{\frac{1}{2}}L_0 \sin\theta}, \tag{A 6}$$

which increases with $x_f$.

As a result, the transition between the gravity-current regime and the turbulent-diffusion regime is not likely to occur during an experiment, and the state of the flow will be determined by the initial conditions.

## Appendix B. Derivation of boundary-layer-averaged equations

For the turbulent boundary layer above the slope, with a constant angle $\theta$, the mean velocity field induced by the buoyant material is given by

$$\frac{\partial u}{\partial t} + u\frac{\partial u}{\partial x} + w\frac{\partial u}{\partial z} = -\frac{1}{\rho_0}\frac{\partial p}{\partial x} + b\sin\theta - \left(\frac{\partial}{\partial x}\overline{u'^2} + \frac{\partial}{\partial z}\overline{u'w'}\right), \tag{B 1}$$

$$\frac{\partial w}{\partial t} + u\frac{\partial w}{\partial x} + w\frac{\partial w}{\partial z} = -\frac{1}{\rho_0}\frac{\partial p}{\partial z} - b\cos\theta - \left(\frac{\partial}{\partial x}\overline{u'w'} + \frac{\partial}{\partial z}\overline{w'^2}\right), \tag{B 2}$$

where the variation in the transverse ($y$) direction has been neglected. It is also assumed that the density variations are small enough to justify the use of the Boussinesq approximation. Here $(u, w)$ and $(u', w')$ are the mean and fluctuating velocity along $(x, z)$, $p$ is the mean pressure, $b$ is the mean buoyancy $(= g(\rho - \rho_0)/\rho_0)$, $\rho$ and $\rho_0$ are mean and reference densities and $g$ is the gravitational acceleration. For turbidity currents, $b$ is equal to $gc(\rho_s - \rho_0)/\rho_0$, where $\rho_s$ and $c$ are the density and the mean concentration of particles, respectively.

Assuming that the boundary-layer approximations ($u \gg w$ and $\partial/\partial x \ll \partial/\partial z$) are satisfied, (B 2) reduces to

$$p = \rho_0 \cos\theta \int_z^\infty b \, \mathrm{d}z. \tag{B 3}$$

Introducing the eddy viscosity to represent the Reynolds stresses, (B 1) becomes

$$\frac{\partial u}{\partial t} + u\frac{\partial u}{\partial x} + w\frac{\partial u}{\partial z} = -\frac{\partial}{\partial x}\int_z^\infty b\cos\theta \, \mathrm{d}z + b\sin\theta + K\left(\frac{\partial^2 u}{\partial x^2} + \frac{\partial^2 u}{\partial z^2}\right), \tag{B 4}$$

where the pressure term is replaced using (B 3).

Equation (B 4) can be integrated in the $z$-direction to yield the following equation:

$$\frac{\partial}{\partial t}\int_0^\infty u \, \mathrm{d}z + \frac{\partial}{\partial x}\int_0^\infty u^2 \, \mathrm{d}z = -\cos\theta \frac{\partial}{\partial x}\int_0^\infty bz \, \mathrm{d}z + \sin\theta \int_0^\infty b \, \mathrm{d}z + K\frac{\partial^2}{\partial x^2}\int_0^\infty u \, \mathrm{d}z - K\left.\frac{\partial u}{\partial z}\right|_{z=0}, \tag{B 5}$$

where viscous friction at $z = 0$ is neglected and the boundary conditions

$$u(z = \infty) = 0, \tag{B 6}$$

$$b(z = \infty) = 0, \tag{B 7}$$

and the conservation of fluid mass

$$\frac{\partial u}{\partial x} + \frac{\partial w}{\partial z} = 0 \tag{B 8}$$

have been used.

Also note that the turbulent Prandtl number has been taken as unity (Tennekes & Lumley 1972). Moreover, it has been assumed that the strong fluctuations in the velocity generated by the wake of the roughness elements exist near the bottom ($z = 0$), since the roughness Reynolds number is much larger than one (i.e. $u_* d/\nu \sim 10^2$, where $u_*$ is the friction velocity; see Tennekes & Lumley 1972). Therefore the viscous friction is negligible at $z = 0$ in comparison with the turbulent friction.

If it is assumed that the parameters $u$ and $b$ maintain approximately similar profiles in the $z$-direction over the height of a buoyant cloud, $h$, as it moves down the slope, they should have the forms

$$u(x, z, t) = U(x, t)\,\zeta_u(\eta), \tag{B 9}$$

$$b(x, z, t) = B(x, t)\,\zeta_b(\eta), \tag{B 10}$$

where

$$\eta = z/h(x, t) \tag{B 11}$$

and $\zeta_u$ and $\zeta_b$ are functions.

The vertical integration of the moments appearing in (B 5) yields

$$\int_0^\infty u\,\mathrm{d}z = Uh \quad \left(\int_0^\infty \zeta_u\,\mathrm{d}\eta = 1\right), \tag{B 12}$$

$$\int_0^\infty b\,\mathrm{d}z = Bh \quad \left(\int_0^\infty \zeta_b\,\mathrm{d}\eta = 1\right), \tag{B 13}$$

$$\int_0^\infty ub\,\mathrm{d}z = UBh \quad \left(\int_0^\infty \zeta_u\zeta_b\,\mathrm{d}\eta = 1\right), \tag{B 14}$$

$$\int_0^\infty u^2\,\mathrm{d}z = S_1U^2h \quad \left(\int_0^\infty \zeta_u^2\,\mathrm{d}\eta = S_1\right), \tag{B 15}$$

$$\int_0^\infty bz\,\mathrm{d}z = S_2Bh^2 \quad \left(\int_0^\infty \eta\zeta_b\,\mathrm{d}\eta = S_2\right), \tag{B 16}$$

where the definitions of $U$, $B$ and $h$ have been employed for (B 12)–(B 14). The quantity $U$, which is defined by (B 13) and (B 14), represents the mean streamwise velocity of the transport of the buoyant cloud The depth-averaged equation then becomes

$$\frac{\partial}{\partial t}(Uh)+\frac{\partial}{\partial x}(S_1U^2h) = -\frac{\partial}{\partial x}(S_2Bh^2\cos\theta)+Bh\sin\theta+K\frac{\partial^2}{\partial x^2}(Uh)-K\left.\frac{\partial U}{Dz}\right|_{z=0}. \tag{B 17}$$

## Appendix C. Relation to the thermal theory

If the pressure and eddy viscosity terms are neglected, (4.1) (or (B 17)) becomes

$$\frac{\partial}{\partial t}(Uh)+2S_1U\frac{\partial}{\partial x}(Uh) = Bh\sin\theta. \tag{C 1}$$

If $S_1 = \frac{1}{2}$, (C 1) can be rewritten as

$$\frac{\mathrm{d}}{\mathrm{d}t}(Uh) = Bh\sin\theta. \tag{C 2}$$

In the thermal model of Beghin *et al.* (1981), $u$ and $b$ are assumed to have the form

$$u = u_0(1+\gamma x'), \tag{C 3}$$

$$b = b_0, \tag{C 4}$$

where $\gamma = (\mathrm{d}L/\mathrm{d}x)/L$, $x' = x-x_0$ when $z < h$, and $x_0-\frac{1}{2}L < x < x_0+\frac{1}{2}L$, and $u = b = 0$ otherwise; here $x_0$ is the centre and $L$ is the horizontal size of the buoyant cloud.

Then the integration of (C 2) can be done using (C 3) and (C 4) to yield

$$\frac{\mathrm{d}}{\mathrm{d}t}(S_3u_0A) = b_0A\sin\theta, \tag{C 5}$$

where

$$S_3 = \int_{-L/2}^{L/2}(1+\gamma x')h\,\mathrm{d}x'\Big/\int_{-L/2}^{L/2}h\,\mathrm{d}x' \tag{C 6}$$

and

$$A = \int_{-L/2}^{L/2}h\,\mathrm{d}x'. \tag{C 7}$$

Note that (C 5) is the same as the expression used in the thermal theory.

## REFERENCES

ALLEN, J. R. L. 1971 Mixing at turbidity current heads, and its geological implication. *J. Sediment. Petrol.* **47**, 97.

BEGHIN, P., HOPFINGER, E. J. & BRITTER, R. E. 1981 Gravitational convection from the instantaneous sources on inclined boundaries. *J. Fluid Mech.* **107**, 407.

ELLISON, T. H. & TURNER, J. S. 1959 Turbulent entrainment in stratified flows. *J. Fluid Mech.* **6**, 423.

FISCHER, H. B., LIST, E. J., KOH, R. C. Y., IMBERGER, J. & BROOKS, N. H. 1979 *Mixing in Inland and Coastal Waters*, Academic.

LINDEN, P. F. & SIMPSON, J. E. 1986 Gravity-driven flows in a turbulent fluid. *J. Fluid Mech.* **122**, 481.

MIDDLETON, G. V. 1966 Experiments on density and turbidity currents: 1. motion of the head. *Can. J. Earth Sci.* **3**, 523.

NOH, Y. & FERNANDO, H. J. S. 1991 Gravity-current propagation along an incline in the presence of boundary mixing. *J. Geophys. Res.* **96**, 12586.

PARKER, G., FUKUSHIMA, Y. & PANTIN, H. M. 1986 Self-accelerating turbidity currents. *J. Fluid Mech.* **171**, 145.

PHILLIPS, O. M., SHYU, J. & SALMUN, H. 1986 An experiment on boundary mixing: mean circulation and transport rates. *J. Fluid Mech.* **173**, 473.

SIMPSON, J. E. 1987 *Gravity Currents in the Environment and Laboratory*. Ellis Horwood.

TENNEKES, H. & LUMLEY, J. L. 1972 *A First Course in Turbulence*. The MIT Press.

THOMAS, N. H. & SIMPSON, J. E. 1985 Mixing of gravity currents in turbulent surroundings: laboratory studies and modelling implications. In *Turbulence and Diffusion in Stable Environments* (ed. J. C. R. Hunt), p. 61. Clarendon.

TURNER, J. S. 1973 *Buoyancy Effects in Fluids*. Cambridge University Press.